Dynamical malaria models reveal how immunity buffers effect of climate variability

Karina Laneri[a,b,1], Richard E. Paul[c,d], Adama Tall[e], Joseph Faye[e], Fatoumata Diene-Sarr[e], Cheikh Sokhna[f], Jean-François Trape[f], and Xavier Rodó[a,g]

[a]Institut Català de Ciències del Clima, Climate Dynamics and Impacts Unit, 08005 Barcelona, Catalonia, Spain; [b]Centro Atómico Bariloche, Consejo Nacional Investigaciones Científicas y Técnicas, Grupo de Física Estadística e Interdisciplinaria, 8400 S. C. de Bariloche, Rio Negro, Argentina; [c]Institut Pasteur, Unité de la Génétique Fonctionnelle des Maladies Infectieuses, Department of Genomes and Genetics, F-75724 Paris cedex 15, France; [d]Centre National de la Recherche Scientifique, Unité de Recherche Associée 3012, F-75015 Paris, France; [e]Institut Pasteur de Dakar, Unité d'Epidémiologie des Maladies Infectieuses (UR 172), BP 220 Dakar, Senegal; [f]Institut de Recherche pour le Développement, Unité de Pathogénie Afro-Tropicale (Unité Mixte de Recherche 198), Département Santé, BP 1386, CP 18524, Dakar, Senegal; and [g]Institució Catalana de Recerca i Estudis Avançats, 08010 Barcelona, Catalonia, Spain

Edited by Burton H. Singer, University of Florida, Gainesville, FL, and approved April 27, 2015 (received for review November 14, 2014)

Assessing the influence of climate on the incidence of *Plasmodium falciparum* malaria worldwide and how it might impact local malaria dynamics is complex and extrapolation to other settings or future times is controversial. This is especially true in the light of the particularities of the short- and long-term immune responses to infection. In sites of epidemic malaria transmission, it is widely accepted that climate plays an important role in driving malaria outbreaks. However, little is known about the role of climate in endemic settings where clinical immunity develops early in life. To disentangle these differences among high- and low-transmission settings we applied a dynamical model to two unique adjacent cohorts of mesoendemic seasonal and holoendemic perennial malaria transmission in Senegal followed for two decades, recording daily *P. falciparum* cases. As both cohorts are subject to similar meteorological conditions, we were able to analyze the relevance of different immunological mechanisms compared with climatic forcing in malaria transmission. Transmission was first modeled by using similarly unique datasets of entomological inoculation rate. A stochastic nonlinear human–mosquito model that includes rainfall and temperature covariates, drug treatment periods, and population variability is capable of simulating the complete dynamics of reported malaria cases for both villages. We found that under moderate transmission intensity climate is crucial; however, under high endemicity the development of clinical immunity buffers any effect of climate. Our models open the possibility of forecasting malaria from climate in endemic regions but only after accounting for the interaction between climate and immunity.

Plasmodium falciparum malaria | immunity | endemicity | climate | vector-borne diseases

Climate plays a key role in driving the seasonal outbreaks of malaria in areas of low or unstable malaria transmission (1–4). Recent studies have shown the possibility of forecasting malaria outbreaks on the basis of climate information and disease features in these low-transmission settings (3, 5). For instance, in highland malaria the role of warming temperatures is vividly debated (4, 6–8) and in desert-epidemic fringes early studies reported predictions of a widespread increase in malaria transmission (9–12). Recent malaria models also predict a global net increase of the population at risk (13); however, others suggest a shift in spatial distribution rather than a large net increase in total malaria incidence worldwide (14, 15). In epidemic fringes, variation in the incidence of disease is largely determined by the seasonal variation of the mosquito population's occurrence and density, which are essentially modulated by local rainfall [e.g., if water limited (3, 16)] or temperature [e.g., if altitude limited (2, 4, 8)]. This is not the case in holoendemic transmission settings, where incidence of disease is determined not only by external forces, but also by the development of clinical and antiparasite immunity. Under intense transmission, clinical immunity develops during childhood after many infections (17, 18), whereby the individual can tolerate nonnegligible parasite densities without showing symptoms. Subsequently, antiparasite immunity, which enables control of parasite density, develops much more slowly (19), leading to a state of premunition, whereby individuals harbor chronic, potentially subpatent infections (20). Continued exposure to the parasite is seemingly required to maintain such premunition (21). Complete protection from further infections is rarely, if ever, achieved. In such high-transmission regions, the relationship between local climate and disease is difficult to disentangle.

In this study, two unique long-term cohort datasets from villages separated by 5 km but with markedly different malaria transmission intensity (Fig. 1, *Upper*) enable us to showcase the relative roles of internal and external factors in malaria epidemiology, assess the potential degree of predictability emanating from climatic variability, and generate estimates of key parameters in determining malaria population dynamics. To this end, we use a recently developed inference methodology for nonlinear stochastic dynamical systems, successfully applied to epidemic dynamics (3, 16) but never applied to endemic settings. A general coupled mosquito–human compartment model that includes possible key mechanisms common to both villages serves our aim of disentangling differences related to immunity, infectivity, superinfection, and asymptomatic infections as well as to measure the relevance of local climate for each village.

Dynamic Malaria Transmission Model

We classify humans into five distinct classes: $S1$, susceptible to infection; E, exposed (i.e., carrying a latent infection but not yet infectious); $I1$, infected symptomatic and infectious; $I2$, infected asymptomatic and infectious; and $S2$, recovered but with a subpatent

Significance

We apply recently developed inference techniques to disentangle the relative impacts of extrinsic climatic and intrinsic immunological forcing on the epidemiology of lethal human malaria, *Plasmodium falciparum*, for two adjacent cohorts in Senegal. For the cohort in which transmission is limited by mosquito existence by rainfall, the pattern of cases is driven by climate forcing. On the contrary, in the village where mosquitoes are present year-round, the impact of climate on incidence is largely buffered by clinical immunity. Our models, which are capable of simulating reported cases over two decades, open the possibility of forecasting malaria from climate in endemic regions but only after accounting for the interaction between climate and immunity.

Author contributions: K.L., R.E.P., A.T., J.F., F.D.-S., C.S., J.-F.T., and X.R. designed research; K.L., R.E.P., A.T., J.F., F.D.-S., C.S., and J.-F.T. performed research; K.L., R.E.P., A.T., J.F., F.D.-S., C.S., and J.-F.T. contributed new reagents/analytic tools; K.L. and X.R. analyzed data; and K.L., R.E.P., and X.R. wrote the paper.

The authors declare no conflict of interest.

This article is a PNAS Direct Submission.

[1]To whom correspondence should be addressed. Email: karinalaneri@gmail.com.

This article contains supporting information online at www.pnas.org/lookup/suppl/doi:10.1073/pnas.1419047112/-/DCSupplemental.

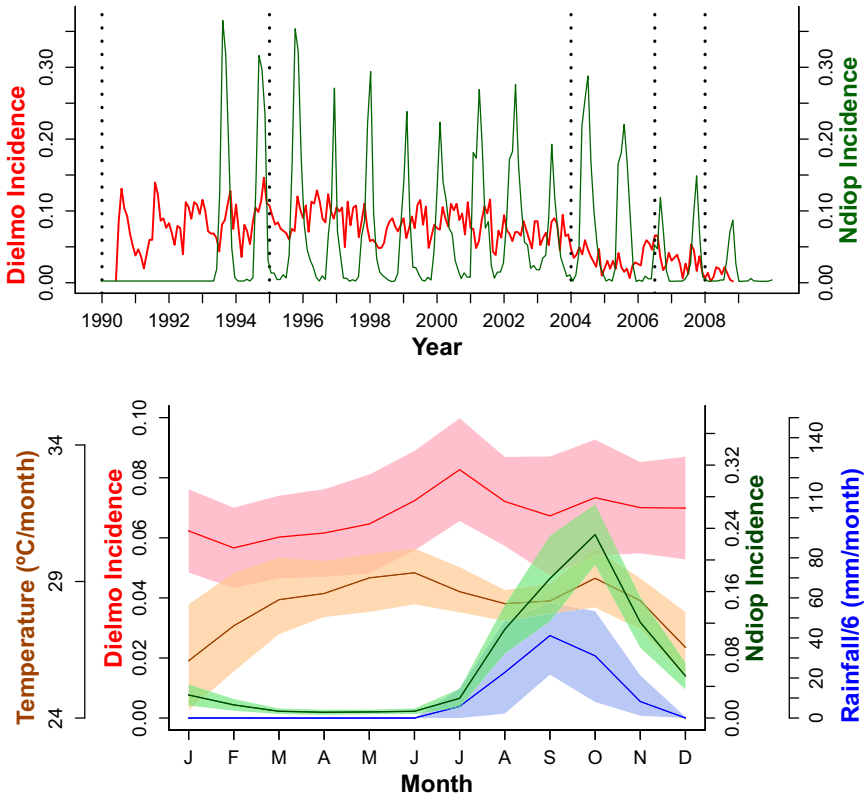

Fig. 1. (*Upper*) *P. falciparum* malaria incidence for Dielmo (red) and Ndiop (green). Vertical dotted black lines separate the four different drug regimes (from left to right: Quinine, Chloroquine, Fansidar, and ACT). Incidence units are episodes per person per month. (*Lower*) Average annual cycles computed as the average month by month for the whole time series of *P. falciparum* monthly incidence for Dielmo (red) and Ndiop (green), local rainfall (blue), and temperature (orange). Shaded regions correspond to the SD.

load of parasites (not completely cleared) and potentially infectious to mosquitoes (Fig. 2). Reinfection, which here includes both superinfections and recrudescent infections that were formerly subpatent, but not new infections, was included as transitions from $S2$ to $I1$ and $I2$ classes. The force of reinfection was considered as a constant proportion, s_i, of the force of infection μ_{S1E} (*SI Text*). Given that the higher the transmission intensity is, the slower the recovery rate (4, 22), immunity and recovery were considered as functions of the transmission intensity as explained in *SI Text*. Drug periods were modeled as constant functions for the corresponding period (see *SI Text* for details), and treatment success probability was considered through a parameter t_s. We do not explicitly model mosquito abundance, survival, or parasite development. Instead, we model vector dynamics through a delayed equation for the force of infection $\mu_{S1E}(t)$, taking into account the fact that the parasite has an extrinsic incubation period, τ, within the mosquito, during which time the parasite passes through its sporogonic cycle (*SI Text*). Transmission was modeled as proportional to the entomological inoculation rate (EIR). Alternatively we replaced mosquito population variability by a set of functions as explained in *SI Text* to account for yearly periodic forces, together with rainfall and temperature anomalies to take into account intrayear variability. The same model was applied to both villages to compare both fitted sets of parameters and infer possible differences in the mechanisms underlying the model. Environmental noise was also included in the transmission term (*SI Text*). We took into account the yearly change in the total human population (Table S1) and the mortality rate was assessed by fitting population data for each of the villages as explained in *SI Text* (see also Fig. S1). Fittings and simulations were performed using open source code for statistical inference for partially observed Monte Carlo processes (23).

Results and Discussion

Plasmodium falciparum incidence time series for Ndiop and Dielmo are shown in Fig. 1, *Upper*. Ndiop, an area with scarce

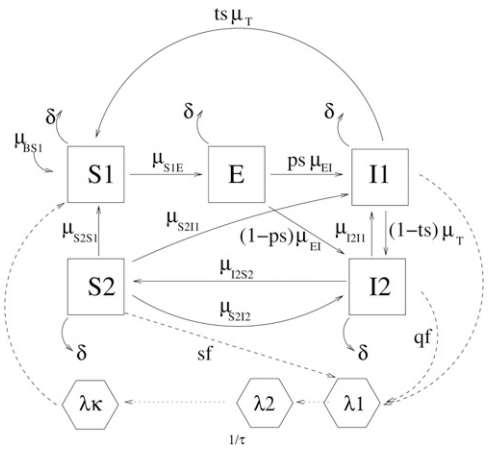

Fig. 2. Flow diagram of the SDE model. Human classes are $S1$ (susceptible), E (exposed, carrying a latent infection), $I1$ (symptomatic infected and infectious), $I2$ (asymptomatic infected and infectious), and $S2$ (recovered subpatent, i.e., having some resistance to reinfection). Mosquito–parasite classes are λ_1 (force of infection at previous time $t - s$) and λ_κ (force of infection at current time t). The possibility of transition between classes X and Y is denoted by a solid arrow, with the corresponding rate written as μ_{XY}. The dotted arrows represent interactions between the human and mosquito stages of the parasite. The model is formalized by Eqs. S1–S5 and Eqs. S9–S11.

vegetation and temporary surface water bodies supplied by seasonal rainfalls (see figure 1, Ndiop, in ref. 24), shows mesoendemic seasonal dynamics. On the contrary, Dielmo, situated on the marshy bank of a small permanent stream (see figure 1, Dielmo, in ref. 24) exhibits perennial malaria transmission leading to a holoendemic type of dynamics. The EIR time series for Dielmo and Ndiop are shown in Fig. S2 classified according to mosquito species. The EIR variability of *Anopheles gambiae sensu lato* is clearly more seasonal than that of *Anopheles funestus* as previously observed (25). Interestingly, there was a significant positive correlation (r_{xy}) between Dielmo cases and Dielmo's EIR of *A. funestus* (Pearson's $r_{xy} = 0.36$, P value $= 2.921e-08$), but not with Dielmo's EIR of *A. gambiae s.l.*. On the contrary for the case of Ndiop there was a significant positive correlation (r_{xy}) between cases and Ndiop's EIR of *A. gambiae s.l.* (Pearson's $r_{xy} = 0.37$, P value $= 3.791e-07$), but not with Ndiop's EIR corresponding to *A. funestus*.

In light of the knowledge about these species' ecology and larval habitat, where *A. gambiae s.l.* breeds in surplus surface water and *A. funestus* prefers to breed in stagnant water at the edge of rivers (25–27), one would expect *A. gambiae s.l.* dynamics to be more dependent on rainfall variability (Fig. S3). We did find a significant correlation between rainfall and Dielmo's EIR of *A. gambiae s.l.* (Pearson's $r_{xy} = 0.42$, P value $= 3.844e-11$) as well as between rainfall and Ndiop's EIR of *A. gambiae s.l.* (Pearson's $r_{xy} = 0.33$, P value $= 3.844e-3$) whereas none was obtained between rainfall and EIR of *A. funestus* either for Dielmo or for Ndiop. It is therefore reasonable to expect that rainfall acts as a pacemaker of *A. gambiae s.l.* population variability affecting in a more direct way Ndiop malaria dynamics.

Averaged malaria incidence in Dielmo and Ndiop together with both mean local rainfall and temperature are shown in Fig. 1, *Lower* (see also Figs. S3 and S4). For the case of Dielmo we observe a steady increase of malaria cases from March, reaching a peak around the month of July, and then staying more or less stationary with barely a second increase in October. This last minor increase in Dielmo agrees with the timing of the Ndiop single peak in malaria cases also occurring around October. Rainfall peaks around August–September and temperature is maximal around the month of July. Therefore, rainfall and temperature are good candidates to influence Ndiop cases variability. However, unlike Ndiop there is no clear picture of the influence of rainfall on the fluctuations of malaria cases in Dielmo's first peak, unless the lower-amplitude anomalies were sufficient to stimulate a large increase in mosquito population and/or to significantly alter EIR values.

We found highly significant correlation values between Ndiop cases and rainfall in the previous month (Pearson's $r_{xy} = 0.75$, P value $= 2.2e-16$), which suggests that rainfall plays an important role in Ndiop malaria dynamics, in agreement with the fact that local climate variability drives malaria outbreaks in low-transmission epidemic fringes (3, 4, 16). In the case of Dielmo, a high-transmission perennial site, the second peak is seen to be significantly modulated by rainfall in the previous month (Dielmo second peak: Pearson's $r_{xy} = 0.24$, P value $= 0.6e-3$) albeit to a lesser extent than in Ndiop. Dielmo's second peak of cases shows a significant negative correlation with temperature (Dielmo second peak: Pearson's $r_{xy} = -0.4$, P value $= 0.7e-10$). Dielmo's first peak of cases is presumably related to the stream dynamics (permanent water availability) and temperature as indicated by the significant correlation with temperature (Dielmo first peak: Pearson's $r_{xy} = 0.36$, P value $= 0.3e-7$) and between *A. funestus* EIR (strongly depending on the stream flow dynamics) and malaria first peak cases in Dielmo (Pearson's $r_{xy} = 0.2$, P value $= 4.4e-3$). All these associations suggest that climate variability plays an important role in malaria dynamics and indicate that climate covariates should be included in the malaria models.

Transmission variability was modeled in four different ways: (*i*) only by means of the EIR, (*ii*) with a seasonal flexible function [seasonal splines (Sp)], and (*iii*) with a combination of a seasonal flexible function and climatic covariate anomalies in two alternative ways [seasonal splines plus linear combination of temperature and rainfall (SpTR)] and SpROT (same as before plus rainfall over temperature) as explained in *SI Text*. Likelihoods of these transmission models for each of the drug periods are shown in Table 1 together with second-order Akaike information criterion (AIC_c) values; AIC_c is a likelihood-based criterion that penalizes for higher number of parameters as well as for size of dataset (28). For both Dielmo and Ndiop the fit improves when rain and temperature anomalies are included in the models (AIC_c values in Table 1 and Tables S2–S4). Values of AIC_c for each of the drug periods (Table 1) show that the average seasonal variation in climate (and therefore in the mosquito population), represented by a flexible function not specified a priori and emerging freely from the fitting procedure, is necessary to describe observed cases. Overall the best performance corresponds to the SpTR model that takes into account rainfall and temperature contributions in a simplest parsimonious way, as an indicator of humidity conditions. The sensitivity of these results with the inclusion of each of the climate covariates is reported in *SI Text*, giving more support to the tight association between rainfall and temperature to fluctuations in mosquito population and parasite development and ultimately to malaria dynamics.

For Dielmo, fitted transmission with the SpTR model exhibits two maxima as shown in Fig. 3. A smallest peak in transmission occurs around June and a second peak in transmission starts to rise in October, reaching its maximum around December. If we accept some seasonality in Dielmo transmission, then people will

Table 1. Maximum likelihood of fits for different drug periods and different transmission dependence

		Ndiop								Dielmo							
		Quinine, $n=26$		Chloroquine, $n=95$		Fansidar, $n=30$		ACT, $n=21$		Quinine, $n=57$		Chloroquine, $n=106$		Fansidar, $n=31$		ACT, $n=27$	
Model	p	ℓ	AIC_c	ℓ	AIC_c	ℓ	AIC_c	ℓ	AIC_c	ℓ	AIC_c	ℓ	AIC_c	ℓ	AIC_c	ℓ	AIC_c
EIR	4	−141	292	−433	874	−143	296	−94	198	−227	463	−398	804	−134	277	−121	252
Sp	3	−113	233	−381	768	−124	255	−90	187	−223	**452**	−399	804	−128	263	−122	251
SpTR	5	−109	**231**	−378	**766**	−121	**254**	−86	**186**	−223	457	−391	**792**	−121	**254**	−115	**243**
SpROT	6	−117	250	−521	1055	−119	**254**	−87	192	−222	458	−392	797	−121	257	−115	246

For each drug period transmission was modeled by means of the entomological inoculation rate (EIR), only with splines (Sp) and with splines and anomalies of rain and temperature (SpTR and SpROT). The p-labeled column corresponds to the number of free parameters. The rest of the parameters were fixed at the maximum-likelihood estimated values listed in Tables S3 and S4. The second-order Akaike information criterion (AIC_c) is computed as $AIC_c = -2\ell + 2p + (2p(p+1))/(n-p-1)$ with n the number of observations. The best fits are shown in boldface type. Overall the fit improves when temperature and rainfall anomalies are considered (SpTR model).

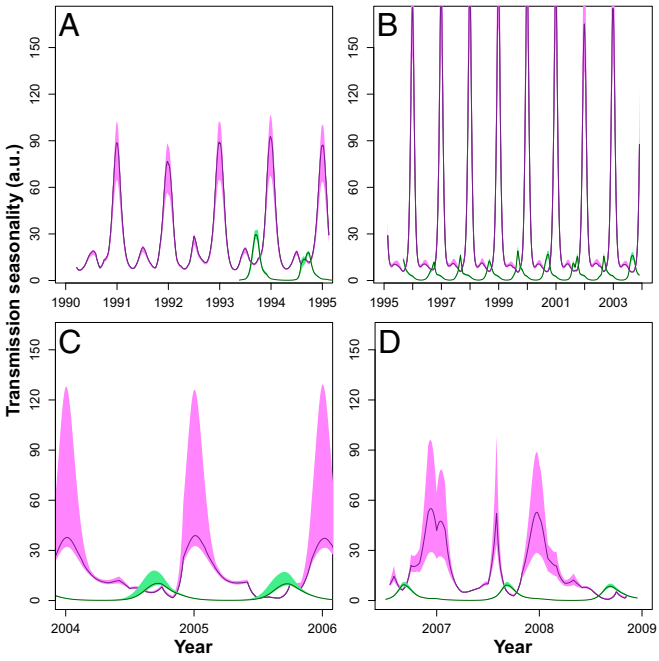

Fig. 3. Fitted transmission seasonality with the SpTR model for each of the drug periods for Dielmo (violet) and Ndiop (green). Lines correspond to the mean of 500 fits, and shaded regions correspond to the 10th and 90th percentiles of all fits. Transmission was modeled as a seasonal spline basis and climatic covariates are explained in *SI Text*. Between years variability in transmission reflects the variability in rainfall and temperature anomalies. (*A*) Quinine period. (*B*) Chloroquine period. (*C*) Fansidar period. (*D*) Artemisinin combination therapies (ACT) period.

have been less exposed to new infections from January to June, losing some short-term clinical immunity and responding more clinically to the rise in infectious bites in July. Following the onset of increased transmission intensity in July (due to the seasonal increase in *A. gambiae s.l.*), by the time December arrives, individuals will have had their clinical immunity boosted by renewed increased exposure to infection and hence have reduced clinical expression. Thus, even when transmission increases in December, the development of short-term clinical immunity would reduce the tendency to have clinical episodes toward the end of the year as can be seen in Fig. 1, *Lower*. For the case of Ndiop, fitted transmission with the SpTR model exhibits a single peak in the seasonal cycle that attains its maximum during August (Fig. 3). According to the SpTR model, transmission intensity is on average 10 times higher in Dielmo (Fig. 3, violet line/shading) than in Ndiop (Fig. 3, green line/shading). This result is independent of our previous knowledge that the number of infectious bites is 10-fold lower in Ndiop than in Dielmo (*SI Text*), validating our modeling approach. School holidays and harvest time coincide with the rainy season and hence lead to temporary intraannual increases in population size, although this variation is minimal and short-lived (Fig. S5) and therefore was not considered in our model.

To be able to compare resulting parameter values between Ndiop and Dielmo, we fitted malaria dynamics of both villages with the same dependence of transmission on climate covariates [as explained in *SI Text* (see also Figs. S6 and S7)]. Parameter values are shown in column SpTR in Tables S3 and S4. Average times from exposed latent to infected were similar in Ndiop and Dielmo ($1/mu_{EI} \approx 10$ d). By contrast, the probability of developing symptoms was much smaller in Dielmo ($P_s \approx 0.04$) than in Ndiop ($P_s \approx 0.8$). To our knowledge, this result is in agreement with a faster development of clinical immunity in Dielmo due to the cumulative exposure to the parasite (29–32). The average time spent as an asymptomatic but infectious individual (t_{I2S2}) is ∼3 mo for Ndiop and 1 mo for Dielmo. In other words, it takes longer to clear the parasite in Ndiop than in Dielmo, reflecting the higher level of antiparasite immunity in the area of higher transmission intensity. Similarly, the time needed to completely clear the parasite (t_{S2S1}) is longer for Ndiop than for Dielmo.

Given that passive as well as active surveillance is performed in both villages (as explained in *SI Text*), all of the infected symptomatic people, i.e., people in the $I1$ class, receive drug treatment. According to our model 90% of the people in $I1$ ($t_s \approx 0.9$) recover in ∼11 d after drug treatment. However, we considered the possibility of drug treatment failure due for example to parasite resistance, in which case it would take between 3 mo and 5 mo to go from the symptomatic ($I1$) to the asymptomatic class ($I2$) without any treatment. This result is in agreement with recent epidemiological observations in sub-Saharan Africa where the average duration of infection was brought down from 270 d to 14 d by administration of drugs (33).

Interestingly for both villages the infectiousness of the asymptomatic ($I2$) and subpatent ($S2$) classes is not negligible (Ndiop, $s_f \approx q_f \approx 0.5$; Dielmo, $s_f \approx 0.6, q_f \approx 0.8$) where the infectivity of the $I1$ class was set to one for comparison. Thus, the proportion of the asymptomatic class infecting mosquitoes is higher in Dielmo than in Ndiop. The reasons for this are not clear, but may reflect differences in the immune state of asymptomatic individuals in the two villages: i.e., despite all broadly belonging to an asymptomatic class, the higher transmission intensity and hence more rapid acquisition of clinical and antiparasite immunity in Dielmo may contribute to differences in infectiousness. Children tend to have

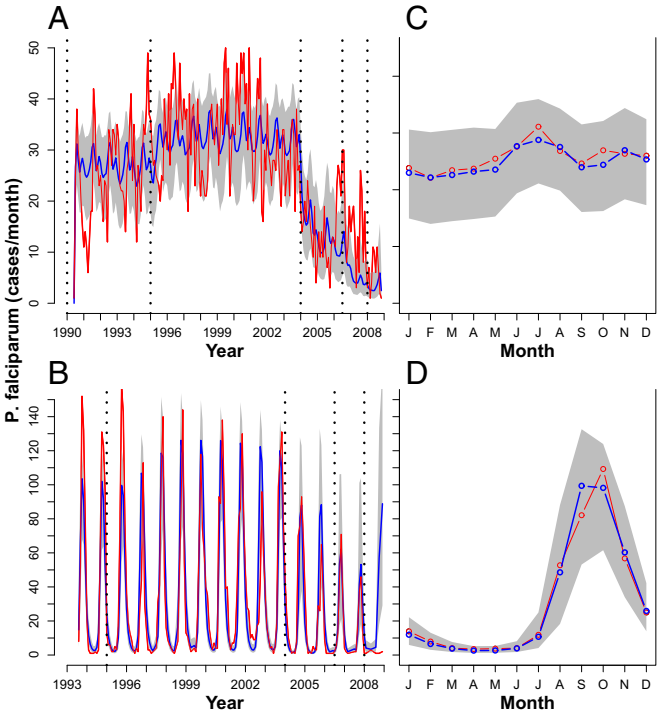

Fig. 4. (*A* and *C*) Dielmo. (*B* and *D*) Ndiop. (*A* and *B*) Red, *P. falciparum cases*; blue, the mean of 1,000 simulations; gray shading, the 10th and 90th percentiles of the simulations. Simulations were done with parameters extracted from 500 fits, weighting them according to their likelihood. All of the simulations were done from the also fitted initial conditions, simulating all of the time series ahead (i.e., with no readjustment of any parameter at any point in time during the simulation). Model used: SpTR. (*A*) Dielmo; (*B*) Ndiop. (*C* and *D*) Monthly average of the curves in *A* and *B*. Simulations are shown in blue/gray and data in red. (*C*) Dielmo; (*D*) Ndiop.

higher gametocyte prevalence rates (34), thus potentially making the younger asymptomatics (in Dielmo) more infectious.

We found that the overall force of reinfection needed for an individual to pass from asymptomatic ($I2$) to symptomatic ($I1$) is comparable between both villages. This result is surprising given that individuals from Dielmo have higher levels of clinical immunity. As for this transition we are taking into account not only superinfection but also recrudescent infections; the use of an age-dependent threshold in Dielmo for asymptomatics may lead to more immediate changes of infected category following superinfection and cumulative parasite densities than in Ndiop. Differences in the parasite density criteria defining the symptomatic class in both villages may likewise lead to a rapid change of state simply on the basis of within-host parasite population dynamics.

Finally, the force of infection needed to change from subpatent ($S2$) to symptomatic ($I1$) in Dielmo is 20 times higher than the one needed in Ndiop. This transition represents pure superinfection in the sense that humans with ultralow parasite densities flip to the symptomatic state. Recent mouse model studies have suggested that superinfection is impaired by the first infection, but only when the blood-stage parasite density exceeds a certain threshold (35); however, the presence of a blood-stage infection can suppress liver-stage immunity (36). Our findings are consistent with these observations. In particular, the force of reinfection needed for transition from subpatent ($S2$) to symptomatic ($I1$) was virtually equal to the overall force of infection in Dielmo. This suggests that subpatent infections in Dielmo are unlikely to recrudesce and generate symptomatic infections, reflecting the high levels of antiparasite and clinical immunity. It is notable that the relative force of infection necessary for the transition from the subpatent to asymptomatic states ($S2$ to $I2$) in Dielmo was lower, consistent with there being greater levels of clinical than antiparasite immunity. In Ndiop, the relative forces of infections necessary for subpatent infections to transit to either asymptomatic or symptomatic infections were similar, confirming our observations on the relative absence of clinical immunity in this population. Notably, however, the presence of an infection or a subpatent infection per se overall increases the risk of a symptomatic (or asymptomatic) infection than if the individual was not infected at all.

Simulations performed for the whole time series period by setting initial conditions and parameters only from the fitting procedure with the SpTR model (Tables S3 and S4) are shown in Fig. 4. Remarkably, they are not next step predictions but 18-y trajectories starting from initial conditions in the 1990s with no posterior readjustment (Fig. 4). In this sense, they reproduce not only the annual average cycles of cases for both villages (Fig. 4, *Lower*), but also the dynamics of the whole time series for both villages (Fig. 4, *Upper*). This remarkable agreement indicates that with the appropriate set of parameters the same structural model can be used to describe Ndiop epidemic as well as Dielmo endemic dynamics.

Conclusions

The implementation of dynamical models in conjunction with recently developed statistical inference methods allowed us to determine some unknown epidemiological malaria parameters as well as to confirm some of the known ones. Furthermore, it enabled us to extract information on important unobserved variables, such as transmission variability, and most significantly to infer the relative importance of different covariates (e.g., climate variability) pertinent to the mechanisms underlying malaria epidemiology. The emerging set of epidemiological parameters consistent with some relevant field observations allowed us to better understand important differences between high- and low-transmission settings, related to parasite immunity, clinical immunity, and reinfection. The dynamic model for *P. falciparum* transmission applied to Dielmo and Ndiop showed that the role of climatic covariates clearly differs in both villages. Whereas in Ndiop rainfall and temperature are key drivers of transmission determining most of the interannual variability in malaria cases, in Dielmo those climate covariates only partially account for the seasonal variation of the force of infection. Climate plays an important role in the increase in malaria cases in Dielmo around July, contributing to the increase in clinical immunity. However, toward the end of the year, clinical immunity reduces the number of clinical cases in the face of an increase in transmission intensity. This new supporting evidence on the interaction between climate and immunity in Dielmo, not observed in Ndiop, suggests for the first time to our knowledge that clinical immunity to malaria might buffer or even halt the effect of climate on transmission intensity in endemic settings in general. For instance, if clinical immunity decreases (e.g., after bed net policies or insecticide campaigns), the distribution of recorded malaria cases throughout the year would change accordingly, making climate and immunity intertwined drivers of variation in incidence of malaria. Recent multimodel approaches addressed the potential expansion of malaria to currently uninfected areas by performing predictions mainly based on climate (13). This study shows that such extrapolation is valid only along the fringes where the disease is unstable but has to be carefully addressed for endemic places where intrinsic factors such as immunity, reinfection, and asymptomatics should be taken into account to reproduce the observed temporal patterns. Our approach opens the possibility to forecast also in malaria endemic regions and could be useful for other datasets from very different epidemiological dynamics as well as for other vector-borne diseases.

Materials and Methods

This program is supported by three different institutions: the Institut Pasteur (Dakar, Senegal), the Institut de Recherche pour le Développement (Marseille, France), and the Senegalese Ministry of Health and Prevention. An agreement between these institutions defines all research activities conducted in this program. The longitudinal surveys were approved by the Ministry of Health of Senegal and the assembled population of the two villages (as explained in *SI Text*). Written informed consent was obtained from all participants. We studied two extensive long-term epidemiological datasets of daily *P. falciparum* confirmed malaria cases, probably among the best malaria records worldwide, recorded for 19 y (1990–2008) in Dielmo and for 16 y (1993–2008) in Ndiop (see *SI Text* for more details) (37). Although these western Senegalese villages are situated only 5 km apart, the epidemiology of both villages is strikingly different. Dielmo village is situated on the marshy bank of a small permanent stream (see figure 1, Dielmo, in ref. 24), where anopheline mosquitoes breed year-round (31, 38) and malaria transmission is intense and perennial, with a mean 258 infected bites per person per year (during 1990–2006) (27). Transmission is on average 10-fold lower in Ndiop (see figure 1, Ndiop, in ref. 24) but highly variable, increasing during the rainy season from July to October (39). Exposure to infection and acquisition of immunity therefore markedly differ in the villages (31, 32, 38, 40). This difference is most evident in the higher *P. falciparum* prevalence rates of infection in Dielmo (80+%) compared with the seasonal rates in Ndiop that change from 20% in the dry season to 70% in the rainy season (31). Mosquitoes of the *A. gambiae s.l.* species complex are the main vectors in both Ndiop and Dielmo. However, notably, *A. funestus* is also present in Dielmo, largely because of the stream that provides a suitable larval habitat. The intensity of malaria transmission was monitored during the whole study period; night-time collections of mosquitoes landing on volunteers were carried out monthly and the sporozoite rate was determined. It was thus possible to estimate the EIR, i.e., the number of infective bites per person per night, for every month of the whole period (see ref. 41 for more information). From 1990 to 2008 four different drug regimes were implemented: Quinine from 1990 to 1994, Chloroquine from 1995 to 2003, Fansidar from 2004 to mid-2006, and Artemisinin-based combination therapy (ACT) from mid-2006 to 2008. Insecticide campaigns were not performed until the implementation of bed nets starting from July 2008 in both villages (37). Rainfall time series from Dielmo (13,685662N, 16,38463W) and Ndiop (13,724620N, 16,409324W) come from a meteorological ground-based manually operated station in each village. Temperature was extracted from National Oceanic and Atmospheric Administration National Climate Data Center Global Hydrology and Climatology Network v2 (42) averaged from the four nearest villages (Cap Skirring, Kaolack, Diourbel, and Ziguinchor).

ACKNOWLEDGMENTS. We thank the villagers of Dielmo and Ndiop for their participation and sustained collaboration in this project, and the field workers (Abdoulaye Badiane, Dominique Manga, Fatou Bintou Badji, Gaoussou Diakhaby, Marie-Louise Senghor, and Roger Ehemba) for their contribution to the project and in generating and maintaining the malaria database. K.L. thanks Gustavo Berman and Hugo Ferrari for kindly allowing the intensive use of the computational resources at Centro Atómico Bariloche for part of this work. X.R. and K.L. were funded by the European Union FP7 Quantifying Weather and Climate Impacts on Health in Developing Countries. X.R. acknowledges the project EUPORIAS (Grant 308291). K.L. is currently a researcher at the National Scientific and Technical Research Council of Argentina.

1. Patz JA, Olson SH (2006) Malaria risk and temperature: Influences from global climate change and local land use practices. *Proc Natl Acad Sci USA* 103(15):5635–5636.
2. Pascual M, Ahumada JA, Chaves LF, Rodó X, Bouma M (2006) Malaria resurgence in the East African highlands: Temperature trends revisited. *Proc Natl Acad Sci USA* 103(15):5829–5834.
3. Laneri K, et al. (2010) Forcing versus feedback: Epidemic malaria and monsoon rains in northwest India. *PLoS Comput Biol* 6(9):e1000898.
4. Alonso D, Bouma MJ, Pascual M (2011) Epidemic malaria and warmer temperatures in recent decades in an East African highland. *Proc Biol Sci* 278(1712):1661–1669.
5. Cash BA, et al. (2013) Malaria epidemics and the influence of the tropical South Atlantic on the Indian monsoon. *Nature Climate Change* 3(5):502–507.
6. Hay SI, et al. (2002) Climate change and the resurgence of malaria in the East African highlands. *Nature* 415(6874):905–909.
7. Zhou G, Minakawa N, Githeko AK, Yan G (2004) Association between climate variability and malaria epidemics in the East African highlands. *Proc Natl Acad Sci USA* 101(8):2375–2380.
8. Siraj AS, et al. (2014) Altitudinal changes in malaria incidence in highlands of Ethiopia and Colombia. *Science* 343(6175):1154–1158.
9. Martens P, et al. (1999) Climate change and future populations at risk of malaria. *Glob Environ Change* 9(Suppl 1):S89–S107.
10. Martens WJ, Niessen LW, Rotmans J, Jetten TH, McMichael AJ (1995) Potential impact of global climate change on malaria risk. *Environ Health Perspect* 103(5):458–464.
11. Martin P, Lefebvre M (1995) *Malaria and Climate: Sensitivity of Malaria Potential Transmission to Climate* (Ambio, Sweden), pp 200–207.
12. Tanser FC, Sharp B, le Sueur D (2003) Potential effect of climate change on malaria transmission in Africa. *Lancet* 362(9398):1792–1798.
13. Caminade C, et al. (2014) Impact of climate change on global malaria distribution. *Proc Natl Acad Sci USA* 111(9):3286–3291.
14. Thomas CJ, Davies G, Dunn CE (2004) Mixed picture for changes in stable malaria distribution with future climate in Africa. *Trends Parasitol* 20(5):216–220.
15. Ermert V, Fink AH, Morse AP, Paeth H (2012) The impact of regional climate change on malaria risk due to greenhouse forcing and land-use changes in tropical Africa. *Environ Health Perspect* 120(1):77–84.
16. Roy M, Bouma M, Ionides E, Dhiman R, Pascual M (2013) The potential elimination of Plasmodium vivax malaria by relapse treatment: Insights from a transmission model and surveillance data from NW India. *PLoS Negl Trop Dis* 7(1):e1979.
17. Doolan DL, Dobaño C, Baird JK (2009) Acquired immunity to malaria. *Clin Microbiol Rev* 22(1):13–36.
18. Snow RW, et al. (1998) Risk of severe malaria among African infants: Direct evidence of clinical protection during early infancy. *J Infect Dis* 177(3):819–822.
19. Marsh K, Snow RW (1997) Host-parasite interaction and morbidity in malaria endemic areas. *Philos Trans R Soc Lond B Biol Sci* 352(1359):1385–1394.
20. Sergent E, Parrot L (1935) L'immunité, la prémunition et la résistance innée [Immunity, premunition and innate resistance]. *Arch Inst Pasteur Alger* 13:279–319. French.
21. Pérignon JL, Druilhe P (1994) Immune mechanisms underlying the premunition against Plasmodium falciparum malaria. *Mem Inst Oswaldo Cruz* 89(Suppl 2):51–53.
22. Filipe JAN, Riley EM, Drakeley CJ, Sutherland CJ, Ghani AC (2007) Determination of the processes driving the acquisition of immunity to malaria using a mathematical transmission model. *PLoS Comput Biol* 3(12):e255.
23. King AA, et al. (2010) *Pomp: Statistical Inference for Partially Observed Markov Processes (R Package) Version 0.43-1* (R Foundation for Statistical Computing, Vienna). Available at pomp.r-forge.r-project.org. Accessed June 5, 2015.
24. Ly AB, et al. (2010) Use of HRP-2-based rapid diagnostic test for Plasmodium falciparum malaria: Assessing accuracy and cost-effectiveness in the villages of Dielmo and Ndiop, Senegal. *Malar J* 9:153.
25. Patz JA, et al. (1998) Predicting key malaria transmission factors, biting and entomological inoculation rates, using modelled soil moisture in Kenya. *Trop Med Int Health* 3(10):818–827.
26. Fontenille D, et al. (1997) High annual and seasonal variations in malaria transmission by anophelines and vector species composition in Dielmo, a holoendemic area in Senegal. *Am J Trop Med Hyg* 56(3):247–253.
27. Bouganali C, et al. (2009) The Dielmo project: An 18-year entomological study of malaria transmission and the bionomics of *Anopheles gambiae* and *Anopheles funestus. 5th MIM Pan-African Malaria Conference, Nairobi, Kenya; Nov 2–6, 2009*. Available at www.mimalaria.org/eng/docs/pdfs/events/Book_of_Abstracts.pdf. Accessed June 5, 2015.
28. Burnham KP, Anderson DR (2004) Multimodel inference: Understanding AIC and BIC in model selection. *Sociol Methods Res* 33:261–304.
29. Rogier C (2000) Natural history of *Plasmodium falciparum* malaria and determining factors of the acquisition of antimalaria immunity in two endemic areas, Dielmo and Ndiop (Senegal). *Bull Mem Acad R Med Belg* 155(5–6):218–226.
30. Rogier C, et al. (1999) *Plasmodium falciparum* clinical malaria: Lessons from longitudinal studies in Senegal. *Parassitologia* 41(1–3):255–259.
31. Sakuntabhai A, et al. (2008) Genetic determination and linkage mapping of *Plasmodium falciparum* malaria related traits in Senegal. *PLoS ONE* 3(4):e2000.
32. Herrant M, et al. (2013) Asthma and atopic dermatitis are associated with increased risk of clinical *Plasmodium falciparum* malaria. *BMJ Open* 3(7):e002835.
33. Águas R, White LJ, Snow RW, Gomes MGM (2008) Prospects for malaria eradication in Sub-Saharan Africa. *PLoS ONE* 3(3):e1767.
34. Beshir KB, et al. (2013) Residual *Plasmodium falciparum* parasitemia in Kenyan children after artemisinin-combination therapy is associated with increased transmission to mosquitoes and parasite recurrence. *J Infect Dis* 208(12):2017–2024.
35. Portugal S, Drakesmith H, Mota MM (2011) Superinfection in malaria: Plasmodium shows its iron will. *EMBO Rep* 12(12):1233–1242.
36. Ocaña-Morgner C, Mota MM, Rodriguez A (2003) Malaria blood stage suppression of liver stage immunity by dendritic cells. *J Exp Med* 197(2):143–151.
37. Loucoubar C, et al. (2011) An exhaustive, non-Euclidean, non-parametric data mining tool for unraveling the complexity of biological systems—novel insights into malaria. *PLoS ONE* 6(9):e24085.
38. Trape JF, et al. (2011) Malaria morbidity and pyrethroid resistance after the introduction of insecticide-treated bednets and artemisinin-based combination therapies: A longitudinal study. *Lancet Infect Dis* 11(12):925–932.
39. Fontenille D, et al. (1997) Four years' entomological study of the transmission of seasonal malaria in Senegal and the bionomics of *Anopheles gambiae* and *A. arabiensis*. *Trans R Soc Trop Med Hyg* 91(6):647–652.
40. Loucoubar C, et al. (2013) High number of previous Plasmodium falciparum clinical episodes increases risk of future episodes in a sub-group of individuals. *PLoS ONE* 8(2):e55666.
41. Cancré N, et al. (2000) Bayesian analysis of an epidemiologic model of *Plasmodium falciparum* malaria infection in Ndiop, Senegal. *Am J Epidemiol* 152(8):760–770.
42. Peterson TC, Russell SV (1997) An overview of the Global Historical Climatology Network temperature data base. *Bull Am Meteorol Soc* 78:2837–2849.

Supporting Information

Laneri et al. 10.1073/pnas.1419047112

SI Text

Cohort Participants, Ethics Approval, and *Plasmodium falciparum* Case Detection and Definition

Participants. The malaria research program involving the inhabitants of the Dielmo and Ndiop villages in Senegal has been ongoing since 1990 as described and documented in detail elsewhere (1–3). Malaria transmission in Ndiop is moderate and strictly seasonal, depending upon the rainy season during the second semester. By contrast, in neighboring Dielmo, the population is exposed to intense, perennial malaria transmission, maintained during the dry season by anopheline production in a stream. The number of infectious bites per person per year, the annual entomological inoculation rate, in Dielmo is of the order of 200 (4), compared with ∼20 in Ndiop (5). This program is supported by three different institutions: the Institut Pasteur (Dakar, Senegal), the Institut de Recherche pour le Développement (IRD) (Marseille, France), and the Senegalese Ministry of Health and Prevention. An agreement between these institutions defines all research activities conducted in this program. A field research station with two dispensaries run by nurses has been constructed for the program, ensuring free-of-charge access to health care for the volunteers. Every villager can join or leave the program at any time and newborns can be included upon the request of their parents or legal guardian, therefore forming an open cohort. In the malaria research program, a family-based longitudinal study is conducted to identify all episodes of fever. Specifically for children under 15 y of age, surveillance is active with a daily visit 6 d/wk (i.e., excluding Sunday) of all of the households by field monitors to detect episodes of fever and related symptoms. In the case of suspected fever or fever-related symptoms, a thick blood smear is systematically performed. After the detailed medical examination has been completed by an experienced health worker, specific treatment is administered. When a clinical malaria attack is diagnosed, an antimalarial treatment is administered according to the National Malaria Control Program guidelines. Presence in the village of each volunteer is also recorded on a daily basis. The longitudinal surveys were approved by the Ministry of Health of Senegal and the assembled population of the two villages. Every year, the program was reexamined by the Conseil de Perfectionnement of the Institut Pasteur in Dakar and the assembled village population; informed consent of the volunteers is renewed every year. More specifically after informing them about the procedures and the purpose of the study, written informed consent was obtained from parents or guardians of children either by signature or by thumbprint on a voluntary consent form written in both French and in Wolof, the main local language. Consent was obtained in the presence of the school director, an independent witness.

***P. falciparum* Life Cycle.** The *Plasmodium* life cycle consists of multiple stages in both human and mosquito hosts. When a (female) mosquito takes a blood meal from an infected human, male and female *Plasmodium* gametocytes may be ingested. Sexual reproduction of the parasite takes place within the mosquito's stomach, forming an ookinete that penetrates the midgut wall and encysts. After a period of 10 d or so, sporozoite-stage parasites emerge from the mature oocyst and migrate to the mosquito's salivary glands. Upon a subsequent blood meal, the sporozoites invade the liver and, after a period of mitotic division, emerge into the blood, reproducing asexually in erythrocytic stages and eventually producing gametocytes to complete the cycle. Immunity to *P. falciparum* is nonsterilizing. After repeated infection, individuals may develop clinical immunity whereby they can tolerate parasites without showing symptoms. Such asymptomatic infections have blood parasite densities that are detectable in a blood smear. Antiparasite immunity, whereby individuals control parasite density, develops more slowly, but complete protection from the parasite is never achieved. Individuals with sufficient antiparasite immunity may be able to control densities below what is detectable by blood smear (although detection can be achieved by molecular methods to a lower density). Without drug treatment, an infection is estimated to last for up to 320 d (6). The model captures some key aspects of the human, parasite, and vector dynamics.

The Model

Our modeling framework was designed to be applicable to both villages. It considers both human and mosquito population variability, the first one through yearly census and the second one either directly from landing catches or indirectly estimated through the variability in local meteorological conditions, mainly local rainfall and temperature. Our model also differs from previous dynamic models applied to Ndiop (7) in that we are fitting both birth and death rates and in that we differentiate humans showing symptoms from asymptomatics (8).

The system of equations for human classes is

$$\frac{dS1}{dt}=\mu_{BS1}N+\frac{dN}{dt}-\mu_{S1E}S1+t_s\mu_T I1+\mu_{S2S1}S2-\delta S1 \qquad \textbf{[S1]}$$

$$\frac{dE}{dt}=\mu_{S1E}S1-\Phi\mu_{EI}E-(1-\Phi)\mu_{EI}E-\delta E \qquad \textbf{[S2]}$$

$$\frac{dI1}{dt}=\Phi\mu_{EI}E-(1-t_s)\mu_T I1+s_{i1}\mu_{S1E}I2+s_{i2}\mu_{S1E}S2-t_s\mu_T I1-\delta I1 \qquad \textbf{[S3]}$$

$$\frac{dI2}{dt}=(1-t_s)\mu_T I1-s_{i1}\mu_{S1E}I2+(1-\Phi)\mu_{EI}E-\mu_{I2S2}I2+s_{i3}\mu_{S1E}S2-\delta I2 \qquad \textbf{[S4]}$$

$$\frac{dS2}{dt}=\mu_{I2S2}I2-\mu_{S2S1}S2-s_{i3}\mu_{S1E}S2-s_{i2}\mu_{S1E}S2-\delta S2, \qquad \textbf{[S5]}$$

where nonlinear terms are highlighted in red and $N(t)$ is the total human population for each village at time t obtained from interpolated yearly census data as shown in Table S1.

The differential Eqs. **S1**–**S5** correspond to a large population limit of homogeneous individual-level models where each individual has exponentially distributed transition times. The birth rate $\mu_{BS1}(t)$ is set to ensure that $S1(t)+S2(t)+E(t)+I1(t)+I2(t)+R(t)=N(t)$ and the death rate was computed by fitting the data as explained in *SI Text*, *Natural Mortality Rate Estimation*).

The force of infection or transmission rate at the current time t is defined as

$$\mu_{S1E}(t)=ba^2c\int_{t_0}^{t}\frac{M(s)}{N(s)}\frac{I(s)}{N(s)}x(s)p(t-s)\,ds \qquad \textbf{[S6]}$$

with $x(s)$, the fraction of uninfected mosquitoes at a previous time s; $M(s)$, total number of mosquitoes at time s; $N(s)$, total number of humans at time s; $I(s)/N(s)$, fraction of infected humans at time s; and $p(.)$, a delay distribution that describes the mosquito

stage of the parasite life cycle and vector survival. We choose $p(.)$ to be a $\Gamma(\kappa, \tau/\kappa)$ density.

Uninfected mosquitoes become infected with malaria with a probability c when they bite (at a rate a) an infected human. The infected mosquitoes then contribute to malaria infection in humans when they again bite an uninfected human (at a rate a) and infect humans with a probability b that has information on immunity.

Instead of explicitly modeling mosquito dependence on the force of infection we can define the transmission rate μ_{S1E} at the current time t in a more general way as

$$\mu_{S1E}(t) = \int_{-\infty}^{t} \lambda(s)\gamma(t-s)d\Gamma(s), \qquad \textbf{[S7]}$$

where $\lambda(s)$ is the force of infection at a previous time s when the mosquito bites the infected human and $\gamma(t-s)$ is a delay distribution (for duration of parasite life cycle inside mosquito plus vector survival).

We take γ to be the density of a $\Gamma(\kappa, \tau/\kappa)$ random variable with mean delay τ and variance τ^2/κ.

Then

$$\gamma(t) = \frac{(\kappa/\tau)^{\kappa} t^{\kappa-1}}{(\kappa-1)!}\exp\{-\kappa t/\tau\}. \qquad \textbf{[S8]}$$

To implement the multiiterated filtering methodology it is necessary to transform the non-Markovian integral **[S7]** in a Markovian chain of differential equations. We consider delay distributions leading to finite-dimensional Markovian representations. The consideration of Gamma-distributed transitions between the latent $\lambda(t)$ and current $\mu_{S1E}(t)$ force of infection replaces the integral and the development–mortality kernel of Eq. **S7** with a series of compartments between μ_{EI} and λ following refs. 9 and 10). We replace the integral **[S7]** by the κ-dimensional Markovian system, $\lambda(t), \ldots \lambda_{\kappa-1}(t), \lambda_{\kappa}(\equiv \mu_{S1E}(t))$:

$$\frac{\lambda_1}{dt} = (\lambda - \lambda_1)\frac{\kappa}{\tau}, \qquad \textbf{[S9]}$$

$$\frac{\lambda_i}{dt} = (\lambda_{i-1} - \lambda_i)\frac{\kappa}{\tau} \quad \text{for } i = 2, \ldots, \kappa-1, \qquad \textbf{[S10]}$$

$$\frac{\mu_{S1E}}{dt} = (\lambda_{\kappa-1} - \mu_{S1E})\frac{\kappa}{\tau}. \qquad \textbf{[S11]}$$

The differential Eqs. **S9–S11** correspond to Gamma-distributed transitions for the latent period of the force of infection. Therefore, Eqs. **S1–S5** for the human population and Eqs. **S9–S11** for the mosquito populations completely determine our coupled human–mosquito malaria model. After experimenting with different choices of κ, we fixed $\kappa = 3$.

Transmission and the Entomological Inoculation Rate

The entomological inoculation rate (EIR) is the number of infectious bites per person per unit time. It can be defined as the product of the human biting rate ($M(t)\,a$) and the sporozoite rate (S).

$$\mathrm{EIR}(t) = M(t)a\,S. \qquad \textbf{[S12]}$$

The human biting rate is the number of bites per human per unit time, where $M(t)$ equals the number of *Anopheles* per person at a given time and a equals the average number of persons bitten by one *Anopheles* in 1 d. The sporozoite rate (S) is the proportion of female mosquitoes containing infective-stage parasites in their salivary glands upon dissection and therefore infectious. Within our framework we could rewrite λ in Eq. **S7** by comparing it with Eq. **S6** as

$$\lambda(t) = \left[\frac{I1(t) + q_f \times I2(t) + s_f \times S2(t)}{N(t)}\exp\{\mathrm{EIR}(t) + D(t)\}\frac{d\Gamma}{dt}\right]\overline{\beta}, \qquad \textbf{[S13]}$$

with $\overline{\beta}$ a dimensional constant set as $\overline{\beta} = yr^{-1}$, which is required to give $\mu_{S1E}(t)$ units of y^{-1}.

Here, q_f and s_f are the fractions of asymptomatics in classes $I2$ and $S2$ respectively capable of infecting mosquitoes, with the fraction of infectives from $I1$ set to 1 for comparison.

Environmental noise was included as multiplicative Gamma noise to take into account the stochasticity that arises from variations in vector abundance and behavior (11, 12). $\Gamma(t)$ denotes a Gamma process with stationary independent increments such that $\Gamma(t) - \Gamma(s) \sim \Gamma([t-s]/\sigma^2, \sigma^2)$, where $\Gamma(a, b)$ is the Gamma distribution with mean ab and variance ab^2. The rationale behind choosing a Gamma noise is that of keeping the term $\lambda(t)$ positive at all times; because a Gamma process is increasing, its derivative ($d\Gamma/dt$) is nonnegative at all times. For the continuous-time process in **[S1–S5]** and **[S9–S11]**, all of the states are necessarily nonnegative. When discretizing to give a Euler solution with time step Δ, this property could be violated. However, with $\Delta = 1$ d, such potential numerical issues did not cause problems in our fitted models.

We modeled drug treatment as a rectangular window function D that is equal to one for the time period of the corresponding drug treatment and zero otherwise. Different drug treatment periods were taken from the dataset:

$$D(t) = \beta_{\mathrm{qui}} D\left[t_{\mathrm{qui}}\right] + \beta_{\mathrm{clo}} D[t_{\mathrm{clo}}] + \beta_{\mathrm{fan}} D\left[t_{\mathrm{fan}}\right] + \beta_{\mathrm{act}} D[t_{\mathrm{act}}]. \qquad \textbf{[S14]}$$

Throughout the text, we refer to this model as the EIR transmission model. The timing of transmission is well emulated by the EIR model for both Dielmo and Ndiop, although not the intensity, a fact that could be due to spatial heterogeneities not taken into account in our model.

Transmission and Climatic Variables

We expect mosquito population $M(s)$ in Eq. **S6** to be seasonal, to have a dependence on climatic factors, and to have a random component. We can rewrite the transmission λ in Eq. **S6** as

$$\lambda(t) = \left[\frac{I1(t) + q_f \times I2(t) + s_f \times S2(t)}{N(t)} \times \exp\left\{\sum_{i=1}^{k}\beta_i s_i(t) + Z(t) + D(t)\right\}\frac{d\Gamma}{dt}\right]\overline{\beta}, \qquad \textbf{[S15]}$$

where $\overline{\beta}$ is a dimensional constant and we set $\overline{\beta} = \mathrm{y}^{-1}$. Here, time is measured in units of years.

Seasonality is modeled nonparametrically through the coefficients $\{\beta_i\}$ of a periodic cubic B-spline basis $s_i(t), i = 1, \ldots, 6$ constructed using six evenly spaced knots. It represents interannual variability in transmission and was modeled by

$$\log \beta_{\mathrm{seas}}(t) = \sum_{i=0}^{5} b_i s_i(t), \qquad \textbf{[S16]}$$

where $s_i(t)$ is a periodic cubic B-spline basis defined so that $s_i(t)$ has a maximum at $t = (2i+1)/12$, and normalized so that $\sum_{i=0}^{5} s_i(t) = 1$. When only splines were considered, we called the model the Sp model.

Time-varying covariates enter via the vector $Z(t)$. Temperature and rainfall variability lead to air and soil moisture fluctuations that drive changes in mosquito population densities and, for temperature, may alter the rate of development of the parasite within the mosquito. In this direction we suggested a (simplest parsimonious) linear combination of temperature and rainfall as an indicator of humidity conditions (SpTR model) as

$$Z(t) = \beta_{\text{rain}} R(t) + \beta_{\text{temp}} T(t), \qquad \textbf{[S17]}$$

where $R(t)$ is the standardized rainfall anomaly and $T(t)$ is the standardized temperature anomaly. All of the climate covariates were normalized to zero mean and unit variance. Therefore, in this model rainfall forcing is represented by the term $\beta_{\text{rain}} R(t)$ and temperature forcing is represented by the term $\beta_{\text{temp}} T(t)$.

The link of the malaria vector breeding sites to land water content (LWC) and/or soil moisture (SM) states in an area has been reported extensively in the past (13). For regions in the world where direct estimates of the local LWC or SM values are lacking, the construction of analogs from rainfall and temperature is justified (14). Soil moisture plays an important role in hydrological processes with partitioning of rainfall into infiltration and runoff or partitioning of net radiation into sensible and latent heat and as such, acting as an analog of the water content remaining in the soil after precipitation. Thus, the combined effect of precipitation and evaporation on SM can be defined as R_k/ET_j with $j = 1, \ldots, k$, where R_k is precipitation of k days ago, and ET_j is evaporation of j days ago. As such, land surface soil moisture integrates the local precipitation and surface evaporation that in subtropical regions is largely dependent on temperature (14). It is well known that there exists a negative correlation between SM states and mean and maximum temperatures, more so in the subtropics and semidesertic areas (15, 16). Eltahir and collaborators (17) also suggested a link between rainfall and surface wet bulb temperature during summer months in the United States, with wet bulb temperature being an indicator of soil moisture (18). Based on these facts we propose an alternative transmission model (SpROT) with an additional term representing the interaction between rainfall and temperature:

$$Z(t) = \beta_{\text{rain}} R(t) + \beta_{\text{temp}} T(t) + \beta_{\text{ROT}} \frac{R(t)}{T(t)}. \qquad \textbf{[S18]}$$

Therefore, the soil moisture term is represented by $\beta_{\text{ROT}} R(t)/T(t)$.

Rainfall time series from Dielmo (13,685662N, 16,38463W) and Ndiop (13,724620N, 16,409324W) come from a meteorological ground-based manually operated station in each village (Fig. S3).

Due to the lack of complete local village data, we averaged the temperature series extracted from the four nearest towns [e.g., Cap Skirring, Kaolack, Diourbel, and Ziguinchor; National Oceanic and Atmospheric Administration (NOAA) National Climate Data Center (NCDC) Global Hydrology and Climatology Network (GHCN) v2] (19). Cap Skirring and Ziguinchor are in Casamance near the border with Guinée Bissau. Diourbel is east of Dakar, in the Sahel region, and Kaolack is the closest town to Dielmo, in between other stations. Maximum, mean, and minimum averaged temperature time series are shown in Fig. S4.

Drug treatment was included as in the previous section through Eq. **S14**.

As described in the main text, the rate of change of the force of infection μ_{S1E} is driven by an exogenous forcing including three sources of variability that influence the vector's abundance and behavior, i.e., seasonality, climate covariates (here, rainfall and temperature), and random noise.

Immunity and Recovery Rates. The rate of loss of immunity from asymptomatics $I2$ to subpatent $S2$ was modeled as dependent on transmission (8, 20, 21),

$$\mu_{I2S2}(t) = \frac{\mu_{S1E}(t)}{e^{\mu_{S1E}(t) t_{I2S2}} - 1},$$

with t_{I2S2} a characteristic time for the transition in the sense that $1/t_{I2S2}$ is the basal rate at which transmission tends to zero. Therefore, t_{I2S2} is expected to be longer in Ndiop than in Dielmo, given the evidence of higher parasite immunity in Dielmo. According to this formulation immunity lasts until the occurrence of a gap of t_{I2S2} mo without exposure. This function is consistent with the fact that in high-transmission places like Dielmo (high μ_{S1E}) the decay of immunity is slower (μ_{I2S2} will be smaller) than in low unstable-transmission sites like Ndiop. Similarly, clearance of subpatent infections was modeled as (20)

$$\mu_{S2S1}(t) = \frac{\mu_{S1E}(t)}{e^{\mu_{S1E}(t) t_{S2S1}} - 1}.$$

This function is consistent with the fact that in high-transmission places like Dielmo (high μ_{S1E}) the process of full recovery is slower than in low unstable-transmission sites like Ndiop.

Superinfection and Recrudescence of Existing Infections. Reinfection from asymptomatic class $I2$ to infected symptomatic $I1$ was considered as a fraction of the force of infection:

$$\mu_{I2I1} = si_1 \mu_{S1E}.$$

This transition takes into account new infections, i.e., superinfection, as well as recrudescent infections. According to our modeling results, even that the fraction of force of infection (relative to that needed to pass from susceptible to exposed) needed for an individual to pass from asymptomatic to symptomatic was much smaller for Dielmo ($si_1 \approx 0.02$) than for Ndiop ($si_1 \approx 0.1$), the forces needed to go from $I2$ to $I1$ are comparable for both villages. This is because the overall force of infection is 10 times higher in Dielmo than in Ndiop.

Superinfection from subpatent infections $S2$ to symptomatic $I1$ was considered as

$$\mu_{S2I1} = si_2 \mu_{S1E}.$$

This transition denotes mainly superinfection in the sense that humans with ultralow parasite densities flip to the symptomatic state.

Reinfection from class $S2$ to class $I2$ was considered as

$$\mu_{S2I2} = si_3 \mu_{S1E}.$$

Our results indicate that the fraction of the force of infection (relative to that needed to pass from susceptible to exposed) resulting in change of state from subpatent to asymptomatic is the same for both villages (0.5); however, as the overall force of infection is 10 times higher in Dielmo than in Ndiop, the total force needed to go from $S2$ to $I2$ is 10 times higher in Dielmo than in Ndiop.

Observation Model. Let C_n be the number of people moving from class E, $S2$, or $I2$ to class $I1$ between time t_{n-1} and t_n, where t_n is the nth observation time; i.e.,

$$C_n = \int_{t_{n-1}}^{t_n} (dN_{EI1}(s) + dN_{S2I1}(s) + dN_{I2I1}(s)).$$

Observations Y_n at time t_n are then modeled as $Y_n | C_n \sim \text{Negbin}(\text{mean} = \rho C_n, \text{var} = \rho C_n + \rho^2 \sigma_{\text{obs}}^2 C_n^2)$. Here ρ is a number

between 0 and 1 that corresponds to the fraction of the infected symptomatic population that reports to the hospital. In our case ρ is expected to be equal to one given that every fever case is diagnosed and, if confirmed, is treated. This fraction was fitted and the obtained values were $\approx$ 0.9 (Tables S3 and S4). The negative binomial distribution accounts for the possibility of overdispersion.

Natural Mortality Rate Estimation

Assuming a population in demographic equilibrium [$\rho_h(\alpha)$ time independent] and ignoring extra mortality due to disease, we can define the density of people ρ_h at a given age α as

$$\rho_h(\alpha) = \delta \frac{e^{-\delta\alpha}}{1 - e^{-\delta\alpha_m}}, \quad \text{[S19]}$$

with δ the natural mortality rate and α_m the maximum age in the human population. Fitted values for the natural mortality rate are shown in Fig. S1 and were set as the fixed value for mortality in the models (i.e., 0.03 1/y).

Population Changes

During the rainy season there is a general return to the village because adolescents and adults return home to help with the harvest. Additionally, is it the holiday period and thus certain children will also return to the village (e.g., those having gone to Koranic school or accompanied adults to towns/cities). In Fig. S5 we compare occupation for both villages during the first (January–June) and second (July–December) semesters of the year. The graph shows the total number of days present cumulative for all villagers during the semester–year for both villages. We see that occupation for both villages does not vary significantly. Although there is a small semestrial increase in the population present in the villages, this is not significant for the overall population or for the child population, which contributes the major part of the clinical episodes. Given that not a clear pattern was observed, this variable was not included in model transmission.

Since the introduction of the on-site medical facility, there has been no mortality due to malaria. Obviously there have been other causes of mortality. The populations are typical of those living in rural malaria endemic regions with (previously) no access to health care. There are no intervillage differences, because living so close (a few kilometers), there is interaction. The only significant behavioral change followed the introduction of bed nets after 2008. There are intraannual population differences but these are small.

Fitted Parameters

We carried out all numerical simulations in the R computing environment, using the R package Pomp (22) to implement the algorithm for statistical inference, which is detailed elsewhere (23, 24). Errors were calculated as a weighted average of all of the fits obtained. The weight assigned to each fit was defined as the normalized likelihood of the fit.

Sensitivity Analysis. To explore the sensitivity of the results to our compound of rainfall and temperature, we also fitted the malaria time series with transmission modeled using temperature and rainfall as separate covariates. We recall here the goodness of fit when taking into account contributions both of rainfall and of temperature in transmission from Tables S3 and S4 (Dielmo, loglik = −782, AIC_c = 1,642; Ndiop, loglik = −631, AIC_c = 1,344). With the combination of splines and temperature (Dielmo, loglik = −784, AIC_c = 1,643; Ndiop, loglik = −634, AIC_c = 1,347) the goodness of fit gets worse than when both contributions are taken into account in transmission. The same happens when a combination of splines and rainfall is considered (Dielmo, loglik = −785, AIC_c = 1,645; Ndiop, loglik = −632, AIC_c = 1,344). Interestingly for the case of Ndiop, accounting for the temperature covariate does not improve significantly the goodness of fit, whereas it does in the case of Dielmo. Rainfall consideration, however, seems to be more crucial to reproduce malaria dynamics in both villages.

Fitting the Malaria Model by Maximum Likelihood. Fitting partially observed nonlinear stochastic dynamic models to data is a methodological challenge. We estimated parameters with a recently developed method, iterated filtering, that allows the likelihood-based comparison of models of disease transmission. This methodology has a plug-and-play property (11, 12), meaning that one needs only to numerically simulate the differential equations that define the model. This enables comparison among a wide class of models. An overview of an iterated filtering procedure, which converges to the maximum of the likelihood function (25, 26), is presented elsewhere (24) where the computationally challenging step is an application of widely used sequential Monte Carlo techniques (27, 28). The method consists of two loops, with the external loop essentially iterating an internal, "filtering" loop and in so doing generating a new, improved estimate of the parameter values at each iteration. The filtering loop implements a selection process for a large number of "particles" over time. For each time step, a particle can be seen as a simulation characterized by its own set of parameter values. Particles can survive or die as the result of a resampling process, with probabilities determined by their likelihood given the data. From this selection process over the whole extent of the data, a new estimate of the parameters is generated, and from this estimate, a cloud of new particles is reinitialized using a given noise intensity adjusted by a cooling factor. This noise, as well as the stochasticity of the dynamics of the system itself, provides the variability for the selection process of the particles to act upon. Further details can be found in refs. 22, 25, and 27–29. Given the huge amount of simulations needed, these computations were done using a cluster for high-performance computing. Fits for Dielmo and Ndiop are shown in Figs. S6 and S7.

1. Trape JF, et al. (1994) The Dielmo project: A longitudinal study of natural malaria infection and the mechanisms of protective immunity in a community living in a holoendemic area of Senegal. *Am J Trop Med Hyg* 51(2):123–137.
2. Rogier C, et al. (1999) *Plasmodium falciparum* clinical malaria: Lessons from longitudinal studies in Senegal. *Parassitologia* 41(1–3):255–259.
3. Trape JF, et al. (2011) Malaria morbidity and pyrethroid resistance after the introduction of insecticide-treated bednets and artemisinin-based combination therapies: A longitudinal study. *Lancet Infect Dis* 11(12):925–932.
4. Fontenille D, et al. (1997) High annual and seasonal variations in malaria transmission by anophelines and vector species composition in Dielmo, a holoendemic area in Senegal. *Am J Trop Med Hyg* 56(3):247–253.
5. Fontenille D, et al. (1997) Four years' entomological study of the transmission of seasonal malaria in Senegal and the bionomics of *Anopheles gambiae* and *A. arabiensis*. *Trans R Soc Trop Med Hyg* 91(6):647–652.
6. Felger I, et al. (2012) The dynamics of natural *Plasmodium falciparum* infections. *PLoS ONE* 7(9):e45542.
7. Cancré N, et al. (2000) Bayesian analysis of an epidemiologic model of *Plasmodium falciparum* malaria infection in Ndiop, Senegal. *Am J Epidemiol* 152(8):760–770.
8. Filipe JAN, Riley EM, Drakeley CJ, Sutherland CJ, Ghani AC (2007) Determination of the processes driving the acquisition of immunity to malaria using a mathematical transmission model. *PLoS Comput Biol* 3(12):e255.
9. Wearing HJ, Rohani P, Keeling MJ (2005) Appropriate models for the management of infectious diseases. *PLoS Med* 2(7):e174.
10. Lloyd AL (2001) Realistic distributions of infectious periods in epidemic models: Changing patterns of persistence and dynamics. *Theor Popul Biol* 60(1):59–71.
11. Bretó C, He D, Ionides EL, King AA (2009) Time series analysis via mechanistic models. *Ann Appl Stat* 3:319–348.
12. He D, Ionides EL, King AA (2010) Plug-and-play inference for disease dynamics: Measles in large and small populations as a case study. *J R Soc Interface* 7(43):271–283.
13. Manguin S, Carnevale P, Mouchet J (2008) *Biodiversity of Malaria in the World* (John Libbey Eurotext, Montrouge, Ile de France, France).
14. Shang KZ, et al. (2007) A scheme for calculating soil moisture content. *Atmos Chem Phys* 7:5197–5206.
15. Karl T (1986) The relationship of soil moisture parameterization to subsequent seasonal and monthly mean temperature in the US. *Bull Am Meteorol Soc* 114: 675–686.

16. Georgakakos K, Bae D, Cayan D (1995) Hydroclimatology of continental watersheds, 1: Temporal analysis. *Water Resour Res* 31(3):655–675.
17. Eltahir E, Pal J (1996) Relationship between surface conditions and subsequent rainfall in convective storms. *J Geophys Res* 101:26337–26345.
18. Findell K, Eltahir E (1997) An analysis of the soil moisture-rainfall feedback, based on direct observations from Illinois. *Water Resour Res* 33:725–735.
19. Peterson TC, Russell SV (1997) An overview of the Global Historical Climatology Network temperature data base. *Bull Am Meteorol Soc* 78:2837–2849.
20. Alonso D, Bouma MJ, Pascual M (2011) Epidemic malaria and warmer temperatures in recent decades in an East African highland. *Proc Biol Sci* 278(1712):1661–1669.
21. Aron JL (1988) Mathematical-modeling of immunity to malaria. *Math Biosci* 90: 385–396.
22. King AA, et al. (2010) *Pomp: Statistical Inference for Partially Observed Markov Processes (R Package) Version 0.43-1* (R Foundation for Statistical Computing, Vienna). Available at pomp.r-forge.r-project.org. Accessed June 5, 2015.
23. Laneri K, et al. (2010) Forcing versus feedback: Epidemic malaria and monsoon rains in northwest India. *PLoS Comput Biol* 6(9):e1000898.
24. Bhadra A, et al. (2011) Malaria in Northwest India: Data analysis via partially observed stochastic differential equation models driven by Lévy noise. *J Am Stat Assoc* 106:440–451.
25. Ionides EL, Bretó C, King AA (2006) Inference for nonlinear dynamical systems. *Proc Natl Acad Sci USA* 103(49):18438–18443.
26. Ionides EL, Bhadra A, Atchadé Y, King AA (2011) Iterated filtering. *Ann Stat* 39: 1776–1802.
27. Doucet A, de Freitas N, Gordon NJ, eds (2001) *Sequential Monte Carlo Methods in Practice* (Springer, New York).
28. Cappé O, Godsill S, Moulines E (2007) An overview of existing methods and recent advances in sequential Monte Carlo. *Proc IEEE* 95:899–924.
29. King AA, Ionides EL, Pascual M, Bouma MJ (2008) Inapparent infections and cholera dynamics. *Nature* 454(7206):877–880.

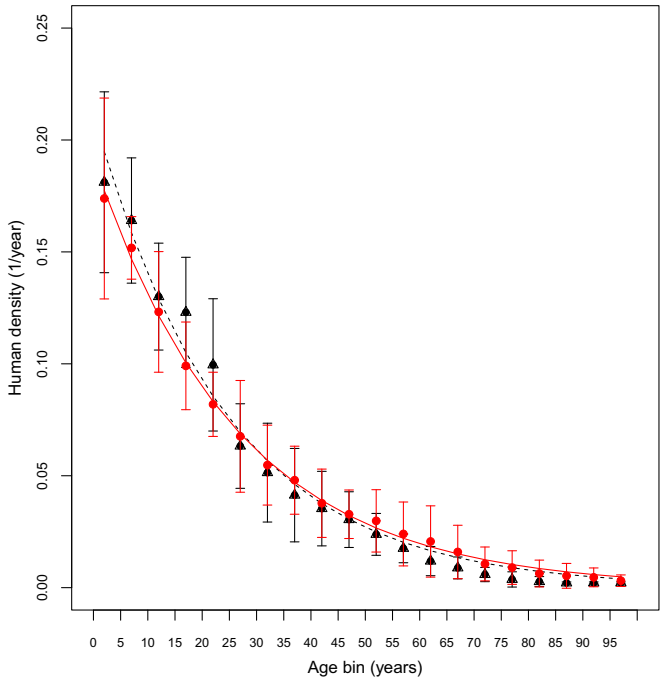

Fig. S1. Age structure and natural mortality rate for Dielmo (red) and Ndiop (black). The average population for each age bin was taken over 15 y for Ndiop (black triangles) and 18 y for Dielmo (red circles); error bars are twice the SD of the mean during those years. Natural mortality rate for Dielmo and Ndiop was fitted according to Eq. **S19**. Fitted values are $\delta = 0.0371/\text{y}$ for Dielmo (red solid line) and $\delta = 0.0411/\text{y}$ for Ndiop (black dotted line).

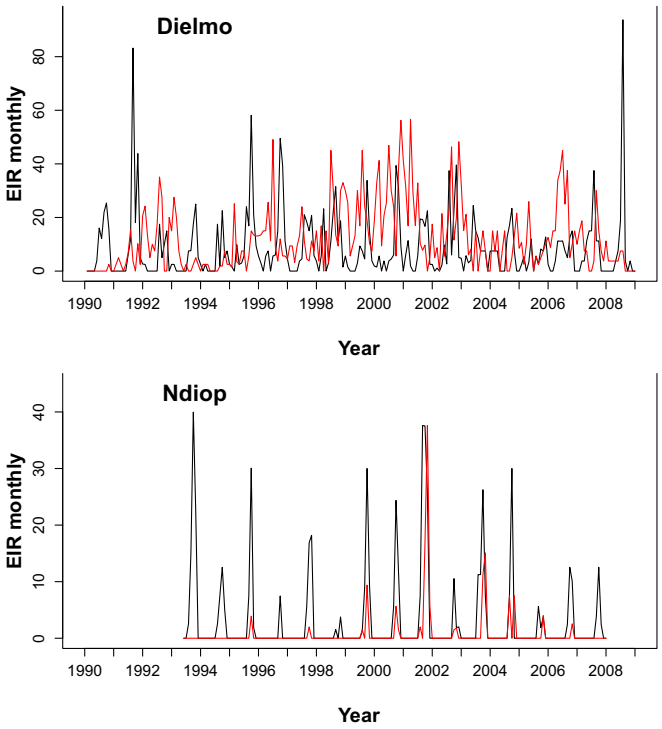

Fig. S2. Monthly entomological inoculation rate (EIR) by mosquito species for Dielmo (*Upper*) and Ndiop (*Lower*). Red lines, *A. funestus*; black lines, *A. gambiae s.l.*

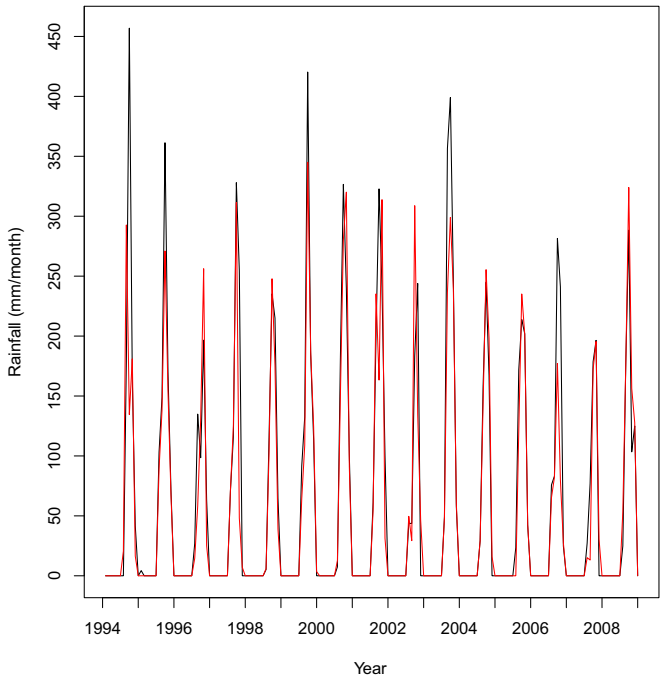

Fig. S3. Monthly rainfall for Ndiop (black) and Dielmo (red). Note the high similarity between rainfall in the two villages.

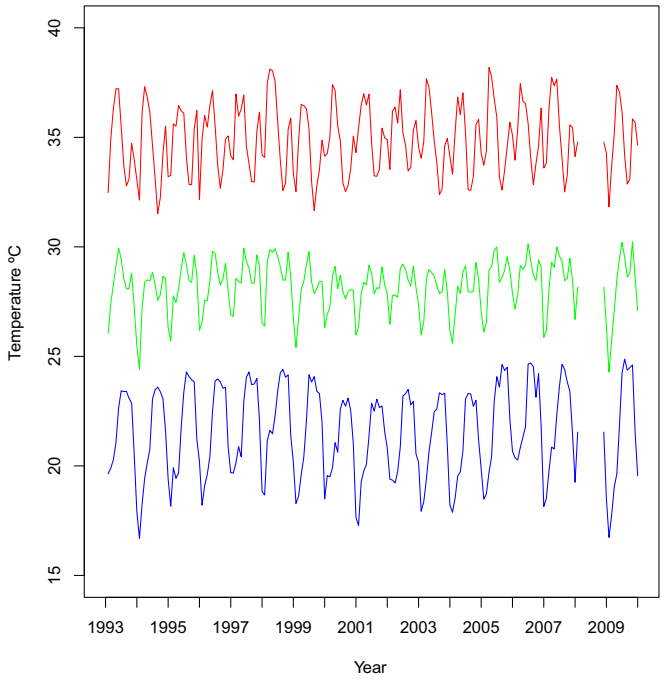

Fig. S4. Maximum (red), mean (green), and minimum (blue) temperature averaged over four locations: Diourbel, Kaolack, Cap Skirring, Ziguinchor. Temperature was extracted from NOAA NCDC GHCN v2 (19).

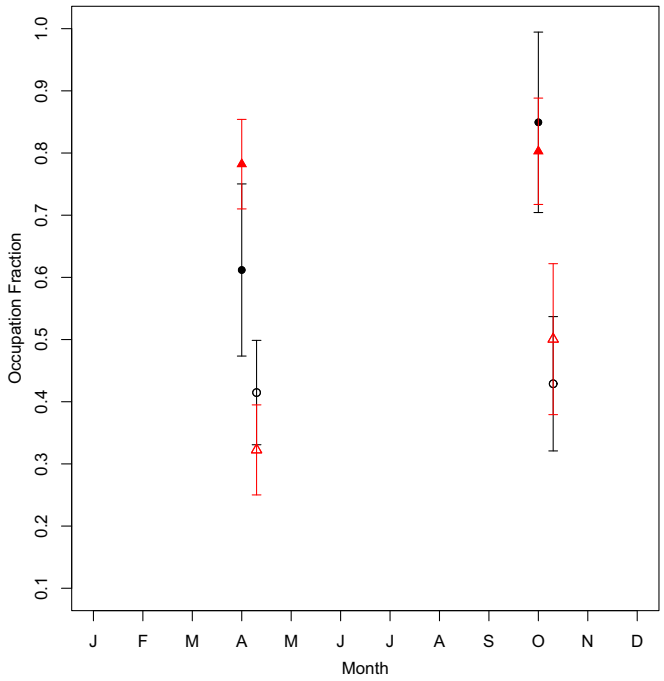

Fig. S5. Occupation fraction for Dielmo (red triangles) and Ndiop (black circles). Solid symbols correspond to all of the population and open symbols correspond to children (less than 15 y old). Mean occupation was calculated as mean number of days present in the village by person during the whole semester. Error bars are the SD of the mean for the 19 y in Dielmo and the 16 y in Ndiop. Mean occupation and error bars are centered on the corresponding semester; they are plotted slightly displaced for clarity.

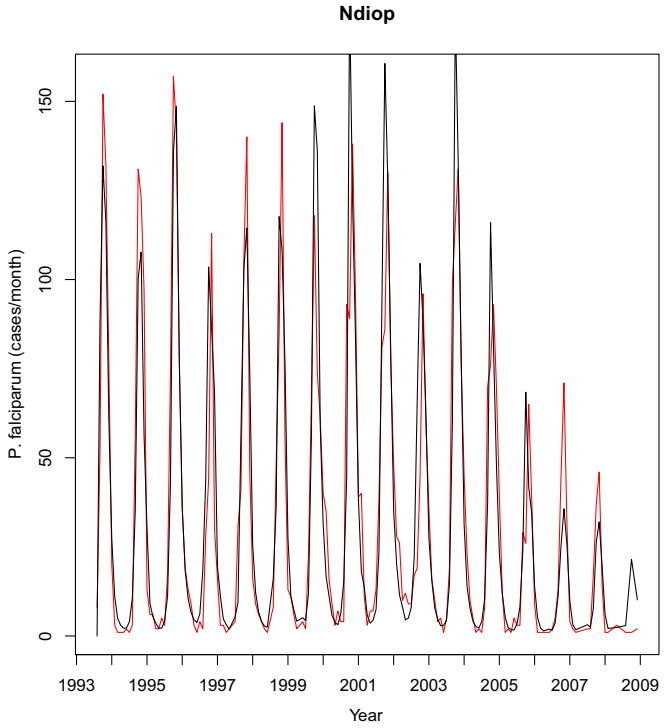

Fig. S6. Ndiop *P. falciparum* time series fitted by multiiterated filtering (MIF) procedure. Transmission was modeled by taking into account different drug periods, seasonal variability, and local climate variability. Population variability was also considered. Model: spTR. Data are shown in red and fit in black.

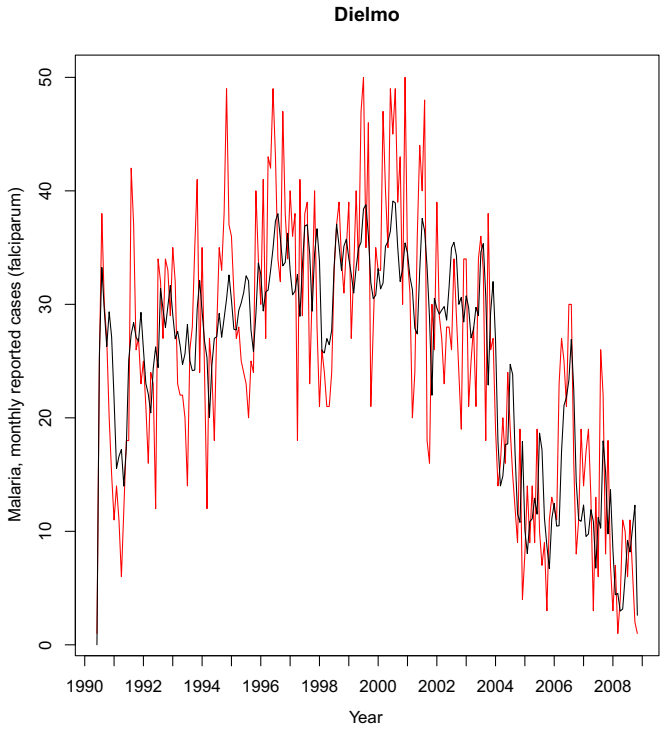

Fig. S7. Dielmo *P. falciparum* time series fitted by multiiterated filtering (MIF) procedure. Transmission was modeled by taking into account different drug periods, seasonal variability, and local climate variability. Population variability was also considered. Model: SpTR. Data are shown in red and fit in black.

Table S1. Population (number of inhabitants) of Ndiop and Dielmo

Village	1990	1991	1992	1993	1994	1995	1996	1997	1998	1999	2000	2001	2002	2003	2004	2005	2006	2007	2008
Dielmo	290	301	303	321	335	333	381	363	434	434	446	414	397	401	405	460	456	487	508
Ndiop	—	—	—	416	414	444	417	476	604	528	513	471	498	455	422	549	477	528	508

Table S2. List of symbols for the malaria model

Symbol	Description	Unit	Estimated? Y/N	Constraints
μ_{XY}	Per-capita rate of transition from compartment X to Y; X, $Y \in \{S1, E, I1, I2, S2\}$	y^{-1}	Y	>0
β_i	Ith spline coefficient	—	Y	None
$\overline{\beta}$	Dimensionality constant	y^{-1}	N	1
τ	Mean development delay for mosquitoes	d	N	11
σ	SD of the process noise	$y^{1/2}$	Y	>0
ρ	Reporting fraction of people in the transition from E to $I1$	—	Y	[0–1]
Δ	Time step for stochastic Euler integration	d	N	1
δ	Natural mortality rate	1/y	N	0.03
σ_{obs}	SD of the observation noise	—	Y	>0
X_0	Initial fraction of people in compartment X; $X \in \{S1, E, I1, I2, S2\}$	—	Y	[0–1]
q_f	Infectivity of asymptomatic people	—	Y	[0–1]
s_f	Infectivity of subpatent infected people	—	Y	[0–1]
ps	Probability of becoming a symptomatic case	—	Y	[0–1]
ts	Fraction of successful treatments	—	Y	[0–1]
si_1	Fraction of force of infection for superinfection (from $I2$ to $I1$)	—	Y	[0–1]
si_2	Fraction of force of infection for superinfection (from $S2$ to $I1$)	—	Y	[0–1]
si_3	Fraction of force of infection for superinfection (from $S2$ to $I2$)	—	Y	[0–1]
β_{rain}	Rainfall coefficient in transmission	—	Y	None
β_{temp}	Temperature coefficient in transmission	—	Y	None
β_{ROT}	Rainfall over temperature coefficient in transmission	—	Y	None
β_{EIR}	Entomological inoculation rate coefficient in transmission	—	Y	>0

Fixed parameters are $\overline{\beta} = 1\ y^{-1}$, $n_\lambda = 2$, $\Delta = 1$ d, $\delta = 0.03\ y^{-1}$, and $ft = 1$.

Table S3. Fitted parameters for Dielmo with transmission modeled as proportional to EIR, with splines, temperature, and rainfall anomalies (SpTR) and with the additional rain over temperature (ROT) term

Description	Symbol	Unit	Dielmo, EIR	Dielmo, SpTR	Dielmo, SpROT
Likelihood	Loglik	—	−800	−782	−783
No. data points	n	—	221	221	221
No. free parameters	p	—	26	33	34
Second-order or corrected Akaike information criteria	AIC_c	—	1,659	1,642	1,646
Time from exposed to infected	$1/\mu_{EI}$	d	15_{1}	13_{4}	13_{3}
Time from symptomatic to asymptomatic	t_{I1I2}	d	146_{36}	109_{30}	109_{15}
Time of immunity decay from asymptomatic to subpatent	t_{I2S2}	d	36_{15}	36_{10}	51_{1}
Time of recovery after treatment	t_{I1S1T}	d	10_{1}	10_{1}	11_{1}
Time of recovery from subpatent infection to susceptible	t_{S2S1}	d	11_{1}	9_{1}	8_{1}
Development time of parasite	τ	d	11	11	11
Measurement noise	σ	—	$0.14_{0.01}$	$0.13_{0.01}$	$0.15_{0.01}$
Observation noise	σ_{obs}	—	$0.02_{0.01}$	$0.03_{0.01}$	$0.04_{0.01}$
Infectivity of *I*2 class	q_f	—	$0.9_{0.1}$	$0.7_{0.1}$	$0.7_{0.1}$
Infectivity of *S*2 class	s_f	—	$0.6_{0.1}$	$0.5_{0.1}$	$0.5_{0.1}$
Reporting rate	ρ	—	$0.98_{0.01}$	$0.99_{0.01}$	$0.99_{0.01}$
Probability of developing symptoms	ps	—	$0.08_{0.01}$	$0.04_{0.02}$	$0.04_{0.01}$
Initial susceptible population	*S*1.0	—	$0.07_{0.01}$	$0.09_{0.04}$	$0.1_{0.2}$
Initial exposed population	*E*.0	—	$0.4_{0.3}$	$0.1_{0.1}$	$0.2_{0.3}$
Initial infected symptomatic population	*I*1.0	—	$0.1_{0.2}$	$0.06_{0.06}$	$0.3_{0.3}$
Initial infected asymptomatic population	*I*2.0	—	$0.4_{0.3}$	$0.09_{0.09}$	$0.4_{0.3}$
Initial susceptible subpatent population	*S*2.0	—	$0.05_{0.05}$	$0.003_{0.003}$	$0.04_{0.1}$
Superinfection fraction, from *I*2 to *I*1	si_1	—	$0.02_{0.01}$	$0.02_{0.01}$	$0.02_{0.01}$
Superinfection fraction, from *S*2 to *I*1	si_2	—	$0.87_{0.1}$	$0.85_{0.01}$	$0.9_{0.01}$
Superinfection fraction, from *S*2 to *I*2	si_3	—	$0.56_{0.1}$	$0.53_{0.01}$	$0.60_{0.05}$
Treatment success	ts	—	$0.94_{0.01}$	$0.91_{0.02}$	$0.91_{0.02}$
EIR coefficient	β_{EIR}	—	$-0.009_{0.001}$	—	—
Rainfall coefficient	β_{rain}	—	—	$-0.07_{0.01}$	$-0.2_{0.08}$
Temperature coefficient	β_{temp}	—	—	$-0.04_{0.01}$	$-0.1_{0.02}$
R over *T* coefficient	β_{ROT}	—	—	—	$0.16_{0.03}$
Drug coefficient Quinine	β_{qui}	—	$1.04_{0.01}$	1.09_{1}	$0.9_{0.1}$
Drug coefficient Chloroquine	β_{clo}	—	$2.9_{0.4}$	2.98_{4}	$3_{0.2}$
Drug coefficient Fansidar	β_{fan}	—	$-0.25_{0.02}$	$-0.19_{0.01}$	$-0.1_{0.01}$
Drug coefficient ACT	β_{act}	—	$-1.27_{0.03}$	$-1.41_{0.02}$	$-1.5_{0.2}$
Spline coefficient	β_1	—	—	$3.3_{0.2}$	$2.2_{0.2}$
Spline coefficient	β_2	—	—	$1.96_{0.02}$	$1.8_{0.2}$
Spline coefficient	β_3	—	—	$1.6_{0.1}$	$1.7_{0.1}$
Spline coefficient	β_4	—	—	$2.72_{0.3}$	$2.8_{0.2}$
Spline coefficient	β_5	—	—	$0.96_{0.02}$	$0.7_{0.1}$
Spline coefficient	β_6	—	—	$2.52_{0.03}$	$2.6_{0.2}$

The number of fitted parameters, including initial conditions, and data points are listed. According to the second-order or corrected Akaike information criteria (AIC_c), the SpTR model better fits the observed data. Subscript numbers are the errors of the fitted parameters.

Table S4. Fitted parameters for Ndiop with transmission modeled as proportional to EIR, with splines, temperature, and rainfall anomalies (SpTR) and with the additional rain over temperature (ROT) term

Description	Symbol	Unit	Ndiop, EIR	Ndiop, SpTR	Ndiop, SpROT
Likelihood	Loglik	—	−737	−631	−631
No. data points	n	—	172	172	172
No. free parameters	p	—	26	33	34
Second-order Akaike information criteria	AIC_c	—	1536	1344	1347
Time from exposed to infected	$1/\mu_{EI}$	d	10_{1}	9_{1}	9_{1}
Time from symptomatic to asymptomatic	t_{I1I2}	d	98_{1}	146_{30}	106_{109}
Time of immunity decay from asymptomatic to subpatent	t_{I2S2}	d	120_{30}	109_{30}	91_{25}
Time of recovery after treatment	t_{I1S1T}	d	31_{6}	11_{1}	11_{1}
Time of recovery from subpatent infection to susceptible	t_{S2S1}	d	109_{30}	109_{30}	109_{33}
Development time of parasite	τ	d	11	11	11
Measurement noise	σ	—	$0.25_{0.02}$	$0.25_{0.02}$	$0.18_{0.01}$
Observation noise	σ_{obs}	—	$0.15_{0.05}$	$0.15_{0.05}$	$0.05_{0.03}$
Infectivity of *I*2 class	q_f	—	$0.6_{0.2}$	$0.5_{0.2}$	$0.7_{0.1}$
Infectivity of *S*2 class	s_f	—	$0.9_{0.2}$	$0.5_{0.2}$	$0.6_{0.1}$
Reporting rate	ρ	—	$0.99_{0.01}$	$0.98_{0.01}$	$0.99_{0.01}$
Probability of developing symptoms	ps	—	$0.6_{0.2}$	$0.8_{0.1}$	$0.7_{0.1}$
Initial susceptible population	*S*1.0	—	$0.3_{0.2}$	$0.7_{0.2}$	$0.7_{0.2}$
Initial exposed population	*E*.0	—	$0.08_{0.02}$	$0.03_{0.02}$	$0.03_{0.02}$
Initial infected symptomatic population	*I*1.0	—	$0.3_{0.01}$	$0.3_{0.3}$	$0.3_{0.2}$
Initial infected asymptomatic population	*I*2.0	—	$0.08_{0.02}$	$0.01_{0.01}$	$0.1_{0.1}$
Initial susceptible subpatent population	*S*2.0	—	$0.3_{0.02}$	$0.02_{0.05}$	$0.04_{0.07}$
Superinfection fraction, from *I*2 to *I*1	si_1	—	$0.7_{0.02}$	$0.1_{0.1}$	$0.14_{0.04}$
Superinfection fraction, from *S*2 to *I*1	si_2	—	$0.1_{0.1}$	$0.4_{0.1}$	$0.5_{0.1}$
Superinfection fraction, from *S*2 to *I*2	si_3	—	$0.1_{0.1}$	$0.5_{0.1}$	$0.6_{0.1}$
Treatment success	ts	—	$0.89_{0.03}$	$0.92_{0.03}$	$0.91_{0.04}$
EIR coefficient	β_{EIR}	—	$9.5_{1.1}$	—	—
Rainfall coefficient	β_{rain}	—	—	$0.008_{0.002}$	$0.08_{0.02}$
Temperature coefficient	β_{temp}	—	—	$-0.5_{0.6}$	$-0.06_{0.04}$
R over *T* coefficient	β_{ROT}	—	—	—	$-0.09_{0.01}$
Drug coefficient Quinine	β_{qui}	—	$2.2_{0.7}$	$0.45_{0.08}$	$0.39_{0.2}$
Drug coefficient Chloroquine	β_{clo}	—	$4.2_{0.8}$	$1.69_{0.01}$	$2.5_{0.3}$
Drug coefficient Fansidar	β_{fan}	—	$0.8_{0.7}$	$-0.4_{0.1}$	$-0.5_{0.2}$
Drug coefficient ACT	β_{act}	—	$0.9_{0.9}$	$-1.23_{0.09}$	$-1.8_{0.2}$
Spline coefficient	β_1	—	—	$0.46_{0.07}$	$0.5_{0.1}$
Spline coefficient	β_2	—	—	$-1.3_{0.1}$	$-1.6_{0.3}$
Spline coefficient	β_3	—	—	$-1.88_{0.03}$	$-1.9_{0.2}$
Spline coefficient	β_4	—	—	$0.5_{0.1}$	$1.1_{0.3}$
Spline coefficient	β_5	—	—	$2.0_{0.3}$	$3.2_{0.2}$
Spline coefficient	β_6	—	—	$0.3_{0.1}$	$0.8_{0.2}$

Number of fitted parameters, including initial conditions, and data points are listed. According to the second-order Akaike information criteria (AIC_c), the SpTR model better fits the observed data. Subscript numbers are the errors of the fitted parameters.